Pressure Dependent Shear Response of Jammed Packings of Frictionless Spherical Particles

Kyle VanderWerf,[1] Arman Boromand,[2] Mark D. Shattuck,[3] and Corey S. O'Hern ![ORCID][2,1,4]

[1]*Department of Physics, Yale University, New Haven, Connecticut 06520, USA*
[2]*Department of Mechanical Engineering & Materials Science, Yale University, New Haven, Connecticut 06520, USA*
[3]*Benjamin Levich Institute and Physics Department, The City College of New York, New York, New York 10031, USA*
[4]*Department of Applied Physics, Yale University, New Haven, Connecticut 06520, USA*

The mechanical response of packings of purely repulsive, spherical particles to athermal, quasistatic simple shear near jamming onset is highly nonlinear. Previous studies have shown that, at small pressure p, the ensemble-averaged static shear modulus $\langle G - G_0 \rangle$ scales with p^α, where $\alpha \approx 1$, but above a characteristic pressure p^{**}, $\langle G - G_0 \rangle \sim p^\beta$, where $\beta \approx 0.5$. However, we find that the shear modulus G^i for an individual packing typically decreases linearly with p along a geometrical family where the contact network does not change. We resolve this discrepancy by showing that, while the shear modulus does decrease linearly within geometrical families, $\langle G \rangle$ also depends on a contribution from discontinuous jumps in $\langle G \rangle$ that occur at the transitions between geometrical families. For $p > p^{**}$, geometrical-family and rearrangement contributions to $\langle G \rangle$ are of opposite signs and remain comparable for all system sizes. $\langle G \rangle$ can be described by a scaling function that smoothly transitions between two power-law exponents α and β. We also demonstrate the phenomenon of *compression unjamming*, where a jammed packing unjams via isotropic compression.

Athermal particulate materials, such as static packings of granular materials [1,2] and collections of bubbles [3] and emulsion droplets [4–6], can jam and develop solidlike properties when they are compressed to packing fractions ϕ above jamming onset. When systems are below jamming onset $\phi < \phi_J$, they possess too few interparticle contacts to constrain all degrees of freedom in the system $N_c < N_c^{\mathrm{iso}}$ [7], and they display fluidlike properties with zero static shear modulus. In systems composed of N spherical particles with purely repulsive interactions, no static friction, and periodic boundary conditions, $N_c^{\mathrm{iso}} = dN' - d + 1$ [8], where d is the spatial dimension, $N' = N - N_r$, and N_r is the number of rattler particles that do not belong to the force-bearing contact network [9]. Several groups have carried out computational studies to understand the structural and mechanical properties of jammed particulate solids with $\phi > \phi_J$ [10–14]. These studies find that the ensemble-averaged contact number $\langle z \rangle = 2\langle N_c \rangle / N$ and static shear modulus $\langle G \rangle$ obey power-law scaling relations in the pressure p as it increases above zero at jamming onset [15]:

$$\langle z \rangle - z^{\mathrm{iso}} \propto \begin{cases} p^\alpha & p < p^* \\ p^\beta & p > p^*, \end{cases} \tag{1}$$

$$\langle G - G_0 \rangle \propto \begin{cases} p^\alpha & p < p^{**} \\ p^\beta & p > p^{**}, \end{cases} \tag{2}$$

where $\langle G_0 \rangle \sim N^{-1}$ is a nonzero constant when the shear modulus is measured at constant volume. The crossover pressures that separate the low and high pressure regimes, $p^* \sim p^{**} \sim N^{-1}$, the scaling exponents, $\alpha \approx 1$ and $\beta \approx 0.5$, are the same for $\langle z \rangle - z^{\mathrm{iso}}$ and $\langle G - G_0 \rangle$, and do not depend sensitively on d and form of the purely repulsive interaction potential [11].

Despite this work, there are many open questions concerning the power-law scaling relations near jamming onset. First, why do the scaling exponents α and β that control the mechanical properties of jammed packings take on their particular values? Studies [16] have suggested that β originates from the near contacts represented in the divergent first peak of the radial distribution function [17] near jamming onset. However, interparticle contacts both form and break as the system is compressed above jamming onset [8]. Second, recent studies [18] have demonstrated the importance of *geometrical families* of jammed packings. Geometrical families are sets of jammed packings that have the same contact network, but possess different packing fractions at jamming onset, and can be continuously transformed into one another via applied deformations. We recently found that the shear modulus of individual jammed packings typically *decreases* with increasing p within geometrical families [19]. This result is at odds with the *ensemble-averaged* behavior, where $\langle G \rangle$ increases with p at nonzero pressures. Thus, additional

studies are required to understand the critical behavior of the mechanical properties of jammed solids near ϕ_J.

Here, we show that the shear modulus G^i for an individual jammed configuration i typically decreases linearly with increasing pressure p as $G^i = G_0^i - \lambda^i p$ along geometrical families, where $\lambda^i > 0$. As p is increased further, one of two things happens: (a) the packing eventually becomes mechanically unstable, and a particle rearrangement occurs, or (b) the packing remains stable, but gains a new contact due to overcompression pushing particles closer together. Both of these events cause a discontinuous jump in G^i. After this jump, the system moves along a new geometrical family as it is compressed until another rearrangement occurs, and this process repeats. We find that the pressure dependence of the ensemble-averaged shear modulus $\langle G \rangle$ is determined by two key contributions: the linear decrease in pressure from geometrical families, and discontinuous jumps from particle rearrangements or added contacts. We identify a physically motivated scaling function that accurately describes $\langle G \rangle$ over a wide range of pressures and system sizes. In addition, we find that jammed packings can *unjam* after applying isotropic compression.

Our derivation of the shear modulus of a single jammed packing undergoing isotropic compression and simple shear along a geometrical family is based on energy conservation: $-pdL^d - \Sigma_{xy} L^d d\gamma = dU$, where L^d is the volume of the simulation cell, γ is the shear strain, and dU is the change in potential energy. Using $dL^d/L^d = -d\phi/\phi$, we find that the shear stress along a geometrical family has two contributions:

$$-\Sigma_{xy} = \frac{1}{L^d}\frac{dU}{d\gamma} - \frac{p}{\phi}\frac{d\phi}{d\gamma}. \qquad (3)$$

The shear modulus is equal to the derivative of $-\Sigma_{xy}$ with respect to γ at constant volume, which gives

$$G^i = \frac{1}{L^d}\frac{d^2U}{d\gamma^2} - \frac{p}{\phi}\frac{d^2\phi}{d\gamma^2}. \qquad (4)$$

Defining $G_0^i \equiv L^{-d} d^2U/d\gamma^2$ and $\lambda^i \equiv \phi^{-1} d^2\phi/d\gamma^2$, we find

$$G^i(p) = G_0^i - \lambda^i p. \qquad (5)$$

Prior results for jammed disk packings have shown that $\lambda^i > 0$ in the limit $p \to 0$ [18]. Here, we study a wide range of pressures and packings of spheres, as well as disks, and find again that $\lambda^i < 0$ is extremely rare. (See Supplemental Material [20].)

We computationally generated packings of frictionless, bidisperse disks and spheres (half large and half small) with a diameter ratio $r = 1.4$ in cubic cells with periodic boundary conditions over a range of system sizes from $N = 6$ to 1024. The particles interact via the purely repulsive linear spring potential:

$$U(r_{ij}) = \frac{\epsilon}{2}\left(1 - \frac{r_{ij}}{\sigma_{ij}}\right)^2 \Theta\left(1 - \frac{r_{ij}}{\sigma_{ij}}\right), \qquad (6)$$

where r_{ij} is the distance between particles i and j, $\sigma_{ij} = (\sigma_i + \sigma_j)/2$, σ_i is the diameter of particle i, ϵ is the characteristic energy scale, and the Heaviside function ensures that particles interact only when they overlap. We measure energy in units of ϵ and stress and shear modulus in units of ϵ/σ_S^d, where σ_S is the diameter of the small particles.

Our first approach to understanding the power-law scaling of the shear modulus is to map out the pressure of individual packings vs ϕ and γ as shown in Fig. 1. Particles are initially placed at random in the simulation cell in the dilute limit at $\gamma = 0$. The system is then compressed in small packing fraction increments. After each step we minimize the total potential energy $U = \sum_{i>j} U(r_{ij})$ with respect to the particle positions using the FIRE algorithm [26] until the system has a total net force satisfying $(\vec{\nabla}U/N)^2 < 10^{-32}$. This initial compression protocol proceeds until $\phi = \phi_i$, where ϕ_i is less than the lowest ϕ_J at $\gamma = 0$ for each system size. After reaching ϕ_i, we generate 10^3 minimized configurations each separated by
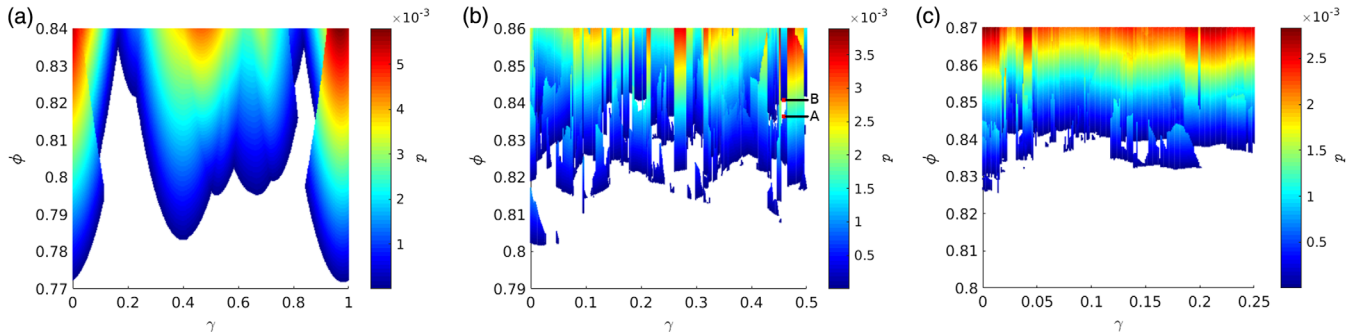

FIG. 1. A contour plot of the pressure p as a function of shear strain γ and packing fraction ϕ originating from a single packing of bidisperse disks with $\gamma = 0$ and the following system sizes and initial packing fractions: (a) $N = 6$, $\phi_i = 0.77$, (b) $N = 32$, $\phi_i = 0.79$, and (c) $N = 64$, $\phi_i = 0.80$. White regions correspond to unjammed packings with $p = 0$, and p increases from dark blue to maroon. In (b), moving from points A to B [i.e., from (0.46,0.837) to (0.46,0.841)] indicates an instance of compression unjamming.
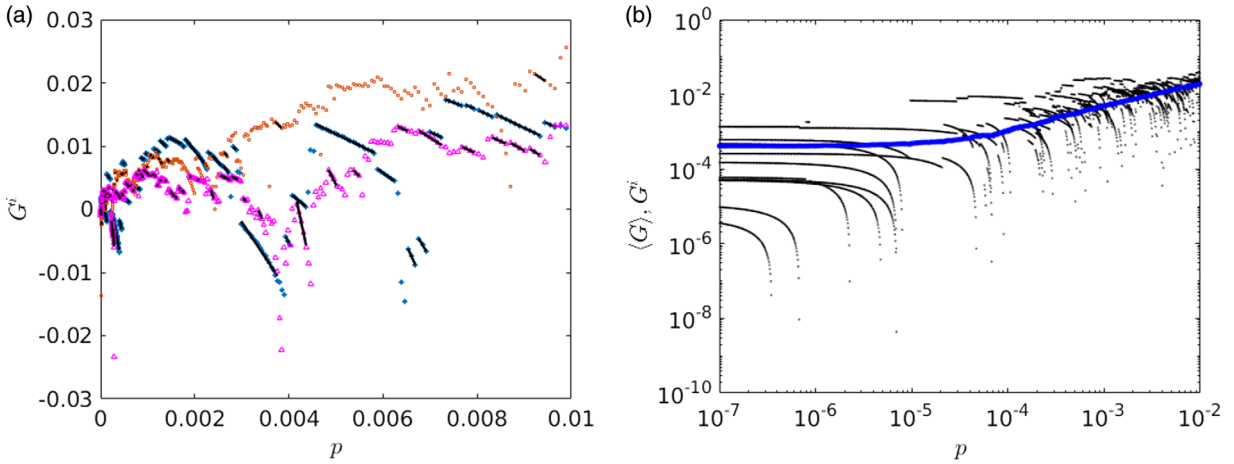
FIG. 2. (a) Shear modulus G^i for individual packings vs pressure p for $N = 64$ (blue asterisks) and 512 (red squares) disks, and 64 spheres (pink triangles). Best-fit lines are plotted in black for some of the geometrical families. Note that some packings are unstable with $G^i < 0$. (b) In black, we plot the shear modulus G^i for ten individual packings of $N = 64$ disks vs p using logarithmic axes. ($G^i < 0$ are omitted.) In blue, we plot the ensemble-averaged shear modulus $\langle G \rangle$ vs p for 5000 packings.

$\Delta\phi = 7 \times 10^{-5}$. Then, we apply an affine simple shear strain to the packing at ϕ_i, such that the new positions satisfy $x_i' = x_i + \Delta\gamma y_i$ with $\Delta\gamma = 10^{-3}$, coupled with Lees-Edwards boundary conditions, followed by energy minimization. We then repeat the compression process at the new value of shear strain.

Figure 1 shows several striking features. First, the ϕ-γ parameter space can be described by smooth, continuous pressure regions corresponding to geometrical families, separated by discontinuous transitions between them. Discontinuities in pressure that occur as a function of ϕ and γ coincide with changes in the interparticle contact network. Second, there are regions where the system is unjammed at a higher packing fraction than a jammed configuration at the same γ. This result implies that it is possible to *unjam* a jammed packing through isotropic compression. See points A and B in Fig. 1(b). This counterintuitive result can be understood from the fact that compression steps change the relative angles between bonds connecting overlapping particle centers. If shifts in the contact network during compression cause a mechanical instability, it can induce a rearrangement to a configuration with a ϕ_J that is larger than the current packing fraction.

Compression unjamming occurs over a range of packing fractions similar to that obtained by quasistatically compressing systems from the dilute limit to jamming onset. It is well known that for this protocol the standard deviation of the distribution of jamming onsets $P(\phi_J)$ narrows as $\Delta \sim N^{-\Omega}$, where $\Omega \sim 0.55$, with increasing N [27]. Even though the length in shear strain of the continuous geometrical families decreases with system size, we find that, for sheared packings, the probability for compression unjamming (averaged over a fixed γ) is independent of system size in the large-N limit. Moreover, we find that for packings generated at fixed $\gamma = 0$ and compressed above

jamming onset, the probability for compression unjamming approaches a nonzero value in the large-N limit. (See Supplemental Material [20].)

To investigate how geometrical families influence the ensemble-averaged shear modulus, we computed G^i vs pressure for N_e jammed disk and sphere packings over a range of system sizes. We varied N_e from 5000 for $N = 64$ to 1000 for $N = 1024$. We generated packings at 10^3 values of p, logarithmically spaced between 10^{-7} and 10^{-2}. To identify rearrangements, we computed the network of force-bearing contacts for every packing at all pressures, using the method described in the Supplemental Material [20].

To determine the shear modulus G^i, we apply positive simple shear strain, typically $N_s = 20$ steps with size $\Delta\gamma = 5 \times 10^{-9}$, each of which is followed by potential energy minimization, to each packing at each p. We have verified that our results for G^i do not depend on the values of N_s and $\Delta\gamma$. To measure linear response even at finite γ, we assume that contacting particles interact via the double-sided linear spring potential [i.e., Eq. (6) without the Heaviside function] and do not include new contacts that form during the applied shear strain. At each γ, we calculate the shear stress using the virial expression [18,28]:

$$\Sigma_{xy} = L^{-d} \sum_{i>j} f_{ijx} r_{ijy}, \qquad (7)$$

where f_{ijx} is the x component of the force on particle i due to particle j, and r_{ijy} is the y component of the separation vector pointing from the center of particle j to the center of i. We fit the shear modulus to a parabolic form in γ, and calculate G^i as $-d\Sigma_{xy}/d\gamma$ evaluated at $\gamma = 0$.

In Fig. 2(a), we show G^i vs p on a linear scale for individual packings of disks and spheres. These results verify the prediction in Eq. (5)—along each geometrical
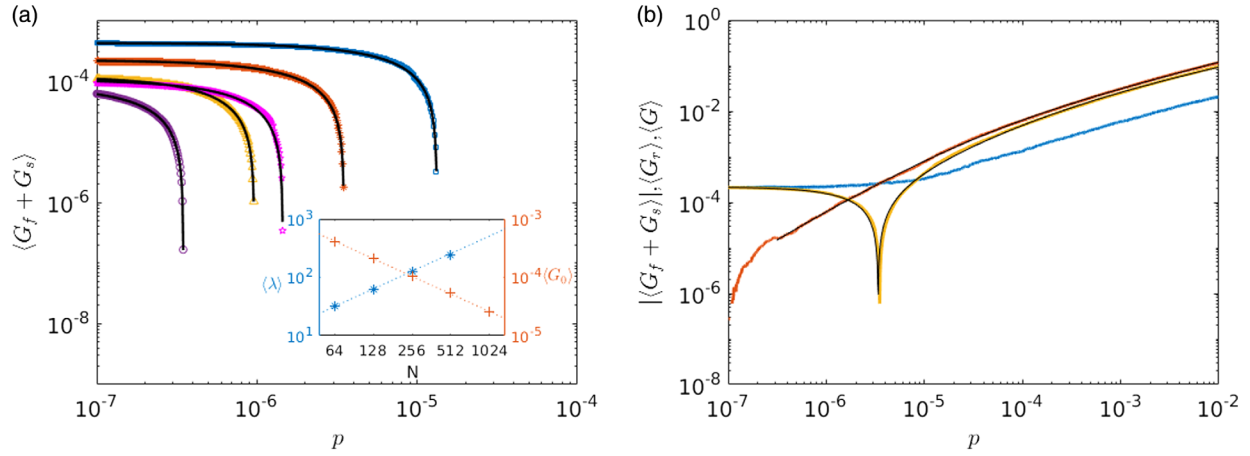
FIG. 3. (a) The sum of the ensemble-averaged first-geometrical-family and change-in-family contributions $\langle G_f + G_s \rangle$ to $\langle G \rangle$ for $N = 64$ (blue squares), 128 (red asterisks), 256 (yellow triangles), and 512 (purple circles) disk packings, and $N = 64$ sphere packings (pink stars). Inset: We fit $\langle G_f + G_s \rangle$ to $\langle G_0 \rangle - \langle \lambda \rangle p$ and show $\langle \lambda \rangle$ (asterisks) and $\langle G_0 \rangle$ (plus signs) for disk packings vs N. (b) For $N = 128$ disks, we plot the absolute value of the sum of the ensemble-averaged first-geometrical-family and change-in-family contributions to $\langle G \rangle$, $|\langle G_f + G_s \rangle|$ (yellow), and ensemble-averaged rearrangement contribution to $\langle G \rangle$, $\langle G_r \rangle$ (red), which are fit to Eqs. (8) and (9), respectively (black). $\langle G \rangle = \langle G_f + G_s + G_r \rangle$ is shown in blue.

family, G^i decreases roughly linearly with p. The regions of linear decreases in p are punctuated by discontinuous jumps in G^i as pressure increases. The jumps in G^i always correspond to either rearrangements in the force-bearing contact network, or added contacts from compression. Figure 2(b), which plots G^i and $\langle G \rangle$ vs p on logarithmic axes, demonstrates that the shear modulus of individual packings can linearly decrease along geometrical families, while at the same time, the ensemble-averaged shear modulus is nearly constant with pressure for small p, and then scales as $p^{1/2}$ at the largest pressures. The discontinuous jumps in G^i from rearrangements give rise, on average, to increases in G^i. Since the jumps in G^i trend upward, they counteract the linearly decreasing behavior of G^i within individual geometrical families, causing a net increase in $\langle G \rangle$ with p for the ensemble average.

To understand the relative contributions of geometrical families and rearrangements to the shear modulus, we decomposed it into three contributions: one from the lowest-pressure (first) geometrical family G_f^i, one from rearrangements G_r^i, and one from changes in the parameters, G_0^i and λ^i, between geometrical families, G_s^i. Hence, $G^i = G_f^i + G_s^i + G_r^i$. We show the ensemble-averaged first-geometrical-family and change-in-family contributions, $\langle G - G_r \rangle = \langle G_f + G_s \rangle$ in Fig. 3(a) for packings of disks and spheres. When the discontinuous jumps are removed, the ensemble-averaged shear modulus decreases linearly with p with slope $\langle \lambda \rangle$ determined by the first geometrical families. Thus, $\langle G_s \rangle \approx 0$ for jammed packings of spherical particles at low pressure. We fit $\langle G_f + G_s \rangle$ to $\langle G_0 \rangle - \langle \lambda \rangle p$, and plot $\langle G_0 \rangle$ and $\langle \lambda \rangle$ vs N in the inset to Fig. 3(a). We find that $\langle G_0 \rangle \sim N^{-1}$, consistent with previous results, and $\langle \lambda \rangle \sim N$.

In Fig. 3(b), we plot the ensemble-averaged $\langle G_r \rangle$, $|\langle G_f + G_s \rangle|$, and $\langle G \rangle$ vs p for $N = 128$ disks. The cusp corresponds to p at which $\langle G_f + G_s \rangle$ switches from positive to negative. For small p, the first-geometrical-family contribution dominates $\langle G \rangle$. At intermediate pressures, $\langle G_f + G_s \rangle \approx 0$, and the rearrangement contribution dominates, $\langle G \rangle \sim \langle G_r \rangle$. However, at the largest pressures, $\langle G_f + G_s \rangle$ is large in magnitude, but negative, and both $\langle G_f + G_s \rangle$ and $\langle G_r \rangle$ determine $\langle G \rangle$. These results hold for all N.

We show that both $\langle G_f + G_s \rangle$ and $\langle G_r \rangle$ are well described by functions that smoothly transition between two power laws as p increases:

$$\langle G_f(p) + G_s(p) \rangle = \langle \bar{G}_0 \rangle + \frac{\bar{a} p^d}{1 + \bar{c} p^{d-e}}, \qquad (8)$$

$$\langle G_r(p) \rangle = \frac{\bar{a}'(p-b)^{d'}}{1 + \bar{c}'(p-b)^{d'-e'}}, \qquad (9)$$

where $\bar{a}$, $\bar{a}'$, $\bar{c}$, and $\bar{c}'$ are positive coefficients, and d, d', e, and e' are positive exponents. We offset $\langle G_r(p) \rangle$ by $b > 0$ in p because $\langle G_r(p) \rangle = 0$ for all pressures below that corresponding to the first rearrangement. We find that the transition between the two power laws (e.g., from exponents d to e) occurs over the same pressure interval for both $\langle G_f + G_s \rangle$ and $\langle G_r \rangle$, which suggests a qualitative change in the nature of rearrangements and potential energy landscape above and below the crossover pressure p^{**}.

After fitting $\langle G_f + G_s \rangle$ and $\langle G_r \rangle$ to Eqs. (8) and (9), we obtain the scaling function for $\langle G \rangle$ by adding the two contributions. However, since $\langle G_f + G_s \rangle$ and $\langle G_r \rangle$ transition between two similar power laws over the same range of p, we
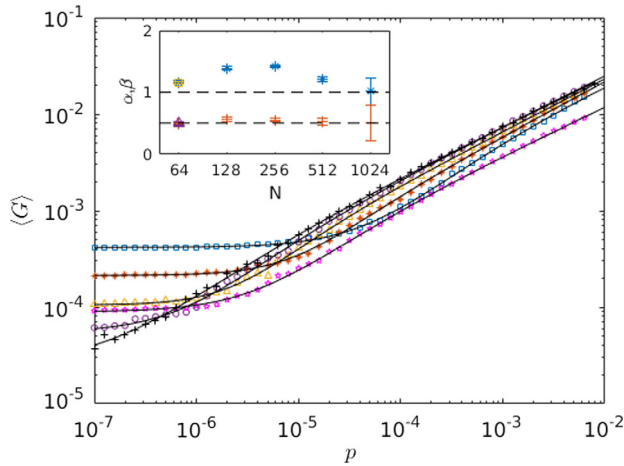
FIG. 4. $\langle G \rangle$ vs p for $N = 64$ (blue squares), 128 (red asterisks), 256 (yellow triangles), 512 (purple circles), and 1024 (black plus signs) disk packings and $N = 64$ sphere packings (pink stars). Each curve except for $N = 1024$ has data at 1000 pressures, but only 50 are shown for clarity. $\langle G \rangle$ is fit to Eq. (8), which interpolates between two power laws with exponents α and $\beta.\alpha$ (asterisks) and β (plus signs) for disk packings are shown vs N in the inset, with error bars given by 95% confidence intervals. The dashed horizontal lines indicate $\alpha = 1$ and $\beta = 0.5$ and the square and triangle correspond to α and β for $N = 64$ sphere packings.

can approximate $\langle G \rangle$ as a single function that transitions between two power laws, rather than a sum of two functions that separately transition between two power laws. Thus, we model $\langle G \rangle$ using Eq. (8), but with different coefficients and exponents: $\langle G \rangle = \langle G_0 \rangle + a p^{\alpha}/(1 + c p^{\alpha-\beta})$. This scaling form is shown on top of the ensemble-averaged $\langle G \rangle$ for jammed disk and sphere packings in Fig. 4, where α and β vs N are given in the inset. As found previously, the exponent that predominates at larger pressures tends toward $\beta = 0.5$, and $\alpha \approx 1$ predominates at lower pressures. The crossover pressure $p^{**} \sim N^{-1}$ decreases with increasing system size.

We have shown that the ensemble-averaged power-law scaling of the shear modulus with pressure p for frictionless spherical particles is a result of two key factors: (a) the shear modulus for each individual packing i decreases linearly with p, $G^i = G_0^i - \lambda^i p$, along geometrical families with fixed contact networks, and (b) discontinuous jumps in G^i that occur when the contact network of a jammed packing changes, and the packing moves to a new geometrical family. The two important contributions to the ensemble-averaged shear modulus, $\langle G_f + G_s \rangle$ and $\langle G_r \rangle$, as well as $\langle G \rangle$, are accurately described by a scaling function that smoothly transitions between two power laws vs p. For $\langle G \rangle$, the exponent $\alpha \approx 1$ at lower pressures and $\beta \approx 0.5$ at higher pressures. Furthermore, we showed that the contributions from geometrical families $\langle G_f + G_s \rangle$ remains important in the large-N limit, because when the contribution of rearrangements is removed, $\langle G \rangle$ linearly decreases with p. Finally, we discovered that jammed

packings can unjam via isotropic compression, which has important implications for studies of reversibility during cyclic compression [29–31].

These results will inspire new investigations of the mechanical response of packings of nonspherical particles. For example, recent computational studies have found that the shear modulus of jammed packings of ellipse-shaped particles scales as $\langle G \rangle \sim p^{\beta}$ with $\beta \approx 1$ [32] in the high-pressure regime, which is different than the scaling exponent found here. Does the presence of quartic vibrational modes [25] change the pressure dependence of rearrangements or geometrical families? Additional studies are required to understand why the power-law scaling of $\langle G \rangle$ with pressure changes with particle shape [33,34]. Prior studies [35] have also shown that $\langle G \rangle$ for frictional sphere packings exhibits similar power-law scaling vs p with $\beta \approx 0.5$ in the large-pressure regime as that found here. Does this occur because frictional interactions do not affect the scaling of $\langle G \rangle$ vs p or is the similarity of the power-law scaling fortuitous? Thus, additional studies are required to understand the pressure-dependent mechanical response of packings of frictional particles.

[1] T. S. Majmudar, M. Sperl, S. Luding, and R. P. Behringer, Phys. Rev. Lett. **98**, 058001 (2007).
[2] R. P. Behringer and B. Chakraborty, Rep. Prog. Phys. **82**, 012601 (2019).
[3] D. J. Durian, Phys. Rev. Lett. **75**, 4780 (1995).
[4] H. P. Zhang and H. A. Makse, Phys. Rev. E **72**, 011301 (2005).
[5] K. W. Desmond, P. J. Young, D. Chen, and E. R. Weeks, Soft Matter **9**, 3424 (2013).
[6] M. Clusel, E. I. Corwin, A. O. N. Siemens, and J. Brujic, Nature (London) **460**, 611 (2009).
[7] A. V. Tkachenko and T. A. Witten, Phys. Rev. E **60**, 687 (1999).
[8] Q. Wu, T. Bertrand, M. D. Shattuck, and C. S. O'Hern, Phys. Rev. E **96**, 062902 (2017).
[9] S. Atkinson, F. H. Stillinger, and S. Torquato, Phys. Rev. E **88**, 062208 (2013).
[10] H. A. Makse, D. L. Johnson, and L. M. Schwartz, Phys. Rev. Lett. **84**, 4160 (2000).
[11] C. S. O'Hern, L. E. Silbert, A. J. Liu, and S. R. Nagel, Phys. Rev. E **68**, 011306 (2003).
[12] C. P. Goodrich, A. J. Liu, and S. R. Nagel, Phys. Rev. Lett. **109**, 095704 (2012).
[13] L. E. Silbert, Soft Matter **6**, 2918 (2010).
[14] S. Henkes, M. van Hecke, and W. van Saarloos, Europhys. Lett. **90**, 14003 (2010).

[15] A. Boromand, A. Signoriello, J. Lowensohn, C. S. Orellana, E. R. Weeks, F. Ye, M. D. Shattuck, and C. S. O'Hern, Soft Matter **15**, 5854 (2019).

[16] A. J. Liu and S. R. Nagel, Annu. Rev. Condens. Matter Phys. **1**, 347 (2010).

[17] L. E. Silbert, A. J. Liu, and S. R. Nagel, Phys. Rev. E **73**, 041304 (2006).

[18] S. Chen, T. Bertrand, W. Jin, M. D. Shattuck, and C. S. O'Hern, Phys. Rev. E **98**, 042906 (2018).

[19] T. Bertrand, R. P. Behringer, B. Chakraborty, C. S. O'Hern, and M. D. Shattuck, Phys. Rev. E **93**, 012901 (2016).

[20] Supplemental Material at http://link.aps.org/supplemental/10.1103/PhysRevLett.124.038004, which includes additional results and Refs. [21–25].

[21] S. Torquato, A. Donev, and F. H. Stillinger, Int. J. Solids Struct. **40**, 7143 (2003).

[22] S. Torquato and F. H. Stillinger, Rev. Mod. Phys. **82**, 2633 (2010).

[23] A. Donev, R. Connelly, F. H. Stillinger, and S. Torquato, Phys. Rev. E **75**, 051304 (2007).

[24] J. N. Roux, Phys. Rev. E **61**, 6802 (2000).

[25] K. VanderWerf, W. Jin, M. D. Shattuck, and C. S. O'Hern, Phys. Rev. E **97**, 012909 (2018).

[26] E. Bitzek, P. Koskinen, F. Gähler, M. Moseler, and P. Gumbsch, Phys. Rev. Lett. **97**, 170201 (2006).

[27] N. Xu, J. Blawzdziewicz, and C. S. O'Hern, Phys. Rev. E **71**, 061306 (2005).

[28] C. P. Goodrich, A. J. Liu, and J. P. Sethna, Proc. Natl. Acad. Sci. U.S.A. **113**, 9745 (2016).

[29] N. Kumar and S. Luding, Granular Matter **18**, 58 (2016).

[30] J. R. Royer and P. M. Chaikin, Proc. Natl. Acad. Sci. U.S.A. **112**, 49 (2015).

[31] Y. Jin, P. Urbani, F. Zamponi, and H. Yoshino, Sci. Adv. **4**, eaat6387 (2018).

[32] C. F. Schreck, N. Xu, and C. S. O'Hern, Soft Matter **6**, 2960 (2010).

[33] H. Jaeger, Soft Matter **11**, 12 (2015).

[34] C. Brito, H. Ikeda, P. Urbani, M. Wyart, and F. Zamponi, Proc. Natl. Acad. Sci. U.S.A. **115**, 11736 (2018).

[35] E. Somfai, M. van Hecke, W. G. Ellenbroek, K. Shundyak, and W. van Saarloos, Phys. Rev. E **75**, 020301(R) (2007).